Pharmacological Characterization and Modeling of the Binding Sites of Novel 1,3-Bis(pyridinylethynyl)benzenes as Metabotropic Glutamate Receptor 5-Selective Negative Allosteric Modulators[S]

Christina Mølck, Kasper Harpsøe, David E. Gloriam, Rasmus P. Clausen, Ulf Madsen, Lars Ø. Pedersen, Hermogenes N. Jimenez, Søren M. Nielsen, Jesper M. Mathiesen, and Hans Bräuner-Osborne

Department of Drug Design and Pharmacology, Faculty of Health and Medical Sciences, University of Copenhagen, Copenhagen, Denmark (C.M., D.E.G., R.P.C., U.M., J.M.M., H.B.-O.); NNF Center for Protein Research, Faculty of Health and Medical Sciences, University of Copenhagen, Copenhagen, Denmark (K.H.); Department for Biologics (L.Ø.P.) and Department of Molecular Pharmacology (S.M.N.), H. Lundbeck A/S, Valby, Denmark; and Department of Chemical and Pharmacokinetic Science, Lundbeck Research USA, Paramus, New Jersey (H.N.J.)

ABSTRACT

Metabotropic glutamate receptor subtype 5 (mGluR5) is a potential drug target in neurological and psychiatric disorders, and subtype-selective allosteric modulators have attracted much attention as potential drug candidates. In this study, the binding sites of three novel 2-methyl-6-(phenylethynyl)pyridine (MPEP)-derived negative allosteric modulators, 2-, 3-, and 4-BisPEB, have been characterized. 2-, 3-, and 4-BisPEB are 1,3-bis(pyridinylethynyl)-benzenes and differ only by the position of the nitrogen atoms in the pyridine rings. Despite their high structural similarity, 2-BisPEB [1,3-bis(pyridin-2-ylethynyl)-benzene, nitrogen atoms in ortho positions], with an IC_{50} value in the nanomolar range, is significantly more potent than the 3- and 4-pyridyl analogs. Mutational analysis, directed by a previously published mGluR5 homology model, was used to determine key residues for the ligand-receptor interactions that may explain the potency differences of 2-, 3-, and 4-BisPEB. Residues Ile651, Pro655, Tyr659, Asn747, Trp785, Phe788, Tyr792, Ser809, and Ala810 were found to have critical roles for the activity of one or more of the three BisPEBs and the reference compound MPEP. The mutagenesis data suggest that the higher potency of 2-BisPEB is due to hydrogen bonding to Ser809 because the S809A mutation made 2-BisPEB equipotent to 3- and 4-BisPEB (IC_{50}, 1–2.5 μM). The potency of MPEP was also greatly affected by S809A (52-fold), suggesting that a Ser809-mediated hydrogen bond is also a key interaction between MPEP and mGluR5. Potential binding modes of 2-, 3-, and 4-BisPEB obtained by molecular docking to the mGluR5 homology model provide a structural context for the reported major mutational effects.

Introduction

Metabotropic glutamate receptors (mGluRs) belong to class C of the G protein-coupled receptor (GPCR) superfamily. They consist of eight subtypes divided into three groups based on sequence similarity, the signal transduction pathway, and pharmacology. They are organized in dimers, and each protomer has a large amino-terminal Venus flytrap domain, encompassing the orthosteric site, connected to the transmembrane domain through a cysteine-rich region (Nakanishi and Masu, 1994; Pin et al., 2003; Bräuner-Osborne et al., 2007; Niswender and Conn, 2010). No drugs directly targeting mGluRs have so far been marketed despite numerous studies supporting the role of mGluRs in several diseases. One example is mGluR subtype 5 (mGluR5), which has been proposed as a target for disorders such as anxiety (Spoo-

ABBREVIATIONS: mGluR, metabotropic glutamate receptor; GPCR, G protein-coupled receptor; mGluR5, metabotropic glutamate receptor subtype 5; 7TMD, 7-transmembrane domain; MPEP, 2-methyl-6-(phenylethynyl)pyridine; NAM, negative allosteric modulator; BisPEB, 1,3-bis(pyridinylethynyl)benzene; BHK cells, baby hamster kidney; ELISA, enzyme-linked immunosorbent assay; ANOVA, analysis of variance; TMH, transmembrane helix.

ren and Gasparini, 2004; Swanson et al., 2005), depression (Palucha and Pilc, 2007), Parkinson's disease (Johnson et al., 2009), and schizophrenia (Conn et al., 2009). Because of a highly conserved orthosteric site (Wellendorph and Bräuner-Osborne, 2009), it has proven difficult to develop potent subtype-selective orthosteric ligands despite the fact that several crystal structures of the Venus flytrap domain are available for several mGluR subtypes [mGluR1 (Kunishima et al., 2000; Tsuchiya et al., 2002), mGluR5 (Protein Data Bank 3LMK), mGluR3, and mGluR7 (Muto et al., 2007)]. As a consequence, efforts have shifted toward the identification of allosteric modulators binding in the less conserved 7-transmembrane domain (7TMD). This has resulted in the identification of several subtype-selective and potent allosteric modulators (Ritzén et al., 2009; Galambos et al., 2010; Zhang et al., 2010).

In addition to being subtype-selective, which in itself is a desired property for drugs, allosteric modulators act by fine-tuning the existing receptor activation because they, in general, do not have intrinsic agonist activity at the wild-type receptor (Goudet et al., 2004; Noetzel et al., 2012). This means that allosteric receptor modulation is dependent on the presence of the endogenous ligand and therefore does not affect the spatiotemporal signal patterns, which is especially important when the highly complex neuronal network of the central nervous system is targeted (Christopoulos et al., 2004; Bridges and Lindsley, 2008; Gregory et al., 2011).

Several class A GPCRs have been cocrystallized with diffusible ligands bound to the 7TMD. The first one was the β_2-adrenergic receptor structure published in 2007 (Cherezov et al., 2007; Rasmussen et al., 2007; Rosenbaum et al., 2007). Since then structures for other receptors, such as β_1-adrenergic (Warne et al., 2008), adenosine A_{2A} (Jaakola et al., 2008), dopamine D_3 (Chien et al., 2010), chemokine CXCR4 (Wu et al., 2010), histamine H_1 (Shimamura et al., 2011), and muscarinic M_2 (Haga et al., 2012), have been determined. However, no crystal structures of the 7TMD of mGluR5 or any other class C GPCRs are available. This fact limits the structural insights into allosteric binding pockets located within the 7TMD and thereby the possibilities for rational discovery and design of new drug candidates. With the lack of target crystal structures, mutational studies combined with homology modeling and/or ligand analog series represent a powerful tool for obtaining important structural information regarding the identity and spatial arrangement of key residues essential for ligand-receptor interactions (Ballesteros and Palczewski, 2001; Gregory et al., 2011). This approach has previously been used for mGluR5 in delineation of the binding site of 2-methyl-6-(phenylethynyl)pyridine (MPEP), a selective negative allosteric modulator (NAM) (Pagano et al., 2000; Malherbe et al., 2003), as well as for other allosteric modulators (Mühlemann et al., 2006; Malherbe et al., 2006; Chen et al., 2007, 2008).

In the present study, mutational analysis, directed by a previously published mGluR5 homology model (Kaae et al., 2012), was used to determine key residues for the ligand-receptor interactions that may explain the potency differences of three novel MPEP-derived NAMs, 2-, 3-, and 4-BisPEB [1,3-bis(pyridin-4-ylethynyl)-benzenes] (Fig. 1). The NAMs were first presented in a recent article by Kaae et al., 2012 in which they were referred to as compounds 19 to 21. These three NAMs only differ in the position of the
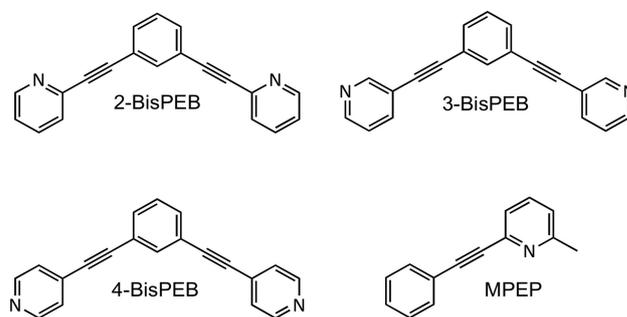

Fig. 1. Chemical structures of the compounds studied: 2-BisPEB [1,3-bis(pyridin-2-ylethynyl)benzene], 3-BisPEB [1,3-bis(pyridin-3-ylethynyl)benzene], 4-BisPEB [1,3-bis(pyridin-4-ylethynyl)benzene], and MPEP [2-methyl-6-(phenylethynyl)pyridine].

nitrogen in the pyridine rings; however, this subtle variation in chemical structure leads to a more than 80-fold potency difference when tested on a stably expressing mGluR5 cell line (Kaae et al., 2012). Uncovering the structural determinants causing the large difference in potency is an important contribution toward understanding the allosteric binding pocket. MPEP was chosen as a reference for mutational studies because this is a well characterized ligand and shares structural elements with the three BisPEBs. Several interacting residues were identified including Ile651, Pro655, Tyr659, Asn747, Trp785, Phe788, Tyr792, Ser809, and Ala810. Mutations of some residues affected all four NAMs, whereas others had differential effects revealing clear differences in NAM-receptor interactions. The mutational analysis was combined with molecular docking to give a structural explanation for the observed potency differences of the three BisPEBs. These results suggest that the potency difference between the three BisPEBs may be explained by a hydrogen bond between 2-BisPEB and Ser809. Ser809 is also suggested to form a strong hydrogen bond to MPEP, a new interaction not previously published as far as we are aware.

Materials and Methods

Materials. 2-, 3-, and 4-BisPEB were synthesized as described previously (Kaae et al., 2012). L-Glutamate and murine anti-FLAG antibody solution (M2) were purchased from Sigma-Aldrich (St. Louis, MO), horseradish peroxidase-conjugated secondary anti-mouse antibody was from Dako (Glostrup, Denmark), Fenobam was acquired from Ascent Scientific (Bristol, UK), MPEP and [^{3}H]MPEP were from Tocris (Bristol, UK) and American Radiolabeled Chemicals (St. Louis, MO), respectively. The Fluo-4 NW Calcium Assay Kit was purchased from Invitrogen (Carlsbad, CA), and bicinchoninic acid assay kits were acquired from Thermo Fisher Scientific (Waltham, MA).

Cell Culturing and Transfection. Baby hamster kidney (BHK) cells were cultured in Dulbecco's modified Eagle's medium with GlutaMAX-I supplemented with 10% diafiltered fetal bovine serum, 100 units/ml penicillin, and 100 μg/ml streptomycin and maintained at 37°C and 5% CO_2. Cells were transiently transfected by the calcium phosphate method at 40 to 60% confluence using 20, 50, and 165 μg of DNA per 100-, 150-, and 245-mm Petri dish, respectively, and a 5- to 6-h incubation at 37°C and 5% CO_2. One day after transfection cells were exposed to G418 either by seeding cells into multiwell plates (for Ca^{2+} mobilization assay and cell surface ELISA) or by changing growth media (for membrane preparation for binding assay) using regular growth media supplemented with 1 mg/ml G418. Ca^{2+} mobilization assays, cell surface ELISA, and membrane preparation were performed 2 days after transfection.

Plasmids and Mutagenesis. The human mGluR5a was tagged with a FLAG epitope (DYKDDDDK) immediately after the signal peptide between amino acids 21 and 22 by overlap polymerase chain reaction to allow for measurement of cell surface expression. The FLAG-tagged mGluR5a was subcloned into pcDNA3.1(+) and used as template for the mutagenesis reactions. Point mutations were generated using 5′-end phosphorylated primers designed according to the principle of the Stratagene QuikChange Multi Site-Directed Mutagenesis Kit or partially overlapping primer pairs designed according to the principle described by Zheng et al. (2004). The genotype of all mutants was confirmed by sequencing by Eurofins MWG Operon (Ebersberg, Germany).

Membrane Preparation and [³H]MPEP Binding Assay. Membranes were prepared [essentially as described previously by Malherbe et al. (2003)] using HEPES-based instead of Tris-based buffers. Membranes were resuspended in binding assay buffer (15 mM Tris-HCl buffer containing 120 mM NaCl, 100 mM KCl, 25 mM CaCl$_2$, and 25 mM MgCl$_2$, pH 7.4, 2.5 μg/ml leupeptin, and 10 μg/ml benzamidine) before freezing in aliquots at −80°C and determining total protein concentration using a bicinchoninic acid assay kit. For binding studies, membranes were thawed and resuspended in binding assay buffer to a final concentration of 20 μg of protein/well. [³H]MPEP, binding assay buffer (total binding), 10 μM fenobam (nonspecific binding), and membranes were mixed for saturation binding. [³H]MPEP, nonradioactive ligand (2-, 3-, and 4-BisPEB), and membranes were mixed for competitive binding studies. Membranes were harvested onto GF/C filters after a 1-h incubation at room temperature as described by Malherbe et al. (2003). Then 40 μl/well scintillation fluid was added, and the filters were counted on a Wallac MicroBeta Trilux (PerkinElmer Life and Analytical Sciences, Waltham, MA) after a 2-h delay minimum. Total radioactivity was measured for each [³H]MPEP concentration on a Tri-Carb liquid scintillation counter (PerkinElmer Life and Analytical Sciences) for calculating the actual concentration as well as evaluating ligand depletion. Ligand depletion (>10%) was observed for some of the lower [³H]MPEP concentrations. However, excluding these points from the data set had no significant effect on graph parameters such as K_d and B_{max}. It was therefore concluded that ligand depletion did not constitute a problem.

Ca²⁺ Mobilization Assay. On the day before the assay, transiently transfected cells were seeded in 96-well plates at 60,000 cells/well using regular growth media supplemented with 1 mg/ml G418. On the day of the assay, cells were incubated at 37°C and 5% CO$_2$ with HEPES buffer (Hanks' balanced salt solution with calcium- and magnesium containing 20 mM HEPES, pH 7.4) supplemented with 1% bovine serum albumin for a minimum of 4 h before dye loading. After the 4-h incubation, cells were washed once with HEPES buffer after which 50 μl/well dye loading solution was added, and cells were incubated for 1 h at 37°C and 5% CO$_2$. The Fluo-4 NW Calcium Assay Kit dye loading solution was prepared by dissolving the content of Component A according to the manufacturer's instructions using probenecid buffer (HEPES buffer supplemented with 2.5 mM probenecid). After dye loading, cells were washed once with probenecid buffer followed by addition of 100 μl/well probenecid buffer and room temperature incubation in the dark for a minimum of 30 min. Glutamate-stimulated increases in intracellular Ca²⁺ concentration were measured on a FDSS7000 imaging-based plate reader (Hamamatsu, Hamamatsu City, Japan) using excitation and emission filters of 480 and 540 nm, respectively.

Cell Surface ELISA. On the day before the assay transiently transfected cells were seeded in poly-D-lysine-coated 48-well plates at 180,000 cells/well using regular growth media supplemented with 1 mg/ml G418. On the day of the assay, cells were washed twice with wash buffer (PBS supplemented with 1 mM CaCl$_2$), followed by a 30-min incubation with blocking solution (50 mM Tris-buffer, pH 7.4, supplemented with 3% bovine serum albumin and 1 mM CaCl$_2$). Blocking solution was replaced by 150 μl/well murine anti-FLAG antibody solution, M2, diluted 1:1000 in blocking solution, and cells

were incubated for 2 h. After incubation, cells were washed 5 times with wash buffer and then incubated for 2 h with 150 μl/well horseradish peroxidase-conjugated secondary anti-mouse antibody, diluted 1:1000 in blocking solution, after which they were washed 5 times with wash buffer. All of the above-mentioned steps were performed at 16–18°C to avoid receptor internalization (von Zastrow and Kobilka, 1994). After the final wash, cells for ELISA measurements were incubated with 230 μl/well 3,3′,5′,5-tetramethylbenzidine for 3 min at room temperature after which 230 μl/well 0.5 N H$_2$SO$_4$ was added to terminate the oxidation of 3,3′,5′,5-tetramethylenbenzidine. Then 200 μl/well was transferred to a clear flat-bottom 96-well plate, and OD$_{450}$ absorbance was read on a Multiskan Ascent (Labsystems, Vienna, VA). Experiments were conducted three to seven times in duplicate. For every plate prepared for ELISA measurements, an identical plate was prepared for protein measurements to evaluate whether mutant expression affected cell viability. These plates were handled in the same way as the ELISA plates except that antibody incubations were replaced with blocking solution incubations. The cells were lysed with 50 to 100 mM NaOH and filtered after the final wash, and total protein concentration of the filtrate was measured using bicinchoninic acid assay kits. We found no significant difference between total protein concentration for cells expressing the wild-type or mutant receptors ($p = 0.32$).

Data Analyses. Prism 5.0a (GraphPad Software Inc., San Diego, CA) was used for data fitting and analysis. Total binding data from saturation binding studies were corrected for nonspecific binding and fitted to the equation: $Y = (B_{max} \times [[^3H]MPEP])/(K_d + [[^3H]MPEP])$ for estimation of K_d. Data from competitive binding studies were fitted to the equation: $Y = \text{bottom} + (\text{top} - \text{bottom})/(1 + 10^{((\log(IC_{50}) - \log([NAM])) \times \text{Hill slope})})$. K_i values for the individual NAMs were calculated from the fitted IC$_{50}$ value and the K_d value of [³H]MPEP, estimated from the saturation binding studies, using the Cheng-Prusoff equation (Cheng and Prusoff, 1973): $K_i = IC_{50}/(1 + [[^3H]MPEP]/K_d)$. Experiments were conducted two to three times in duplicate.

Data from glutamate concentration-response experiments were normalized and fitted to $Y = \text{bottom} + (\text{top} - \text{bottom})/(1 + 10^{((\log(EC_{50}) - [\text{glutamate}]) \times \text{Hill slope})})$. Data from NAM concentration-response experiments were normalized and fitted to $Y = \text{bottom} + (\text{top} - \text{bottom})/(1 + 10^{((\log(IC_{50}) - \log([NAM])) \times \text{Hill slope})})$. Experiments were conducted 2 to 19 times in duplicate. Mutants were compared with the wild type using a one-sample t test (for mutants with NAM IC$_{50}$ ≥45 μM, the highest possible concentration due to solubility issues) or one-way ANOVA followed by Dunnett's multiple comparison test.

Molecular Docking. 2-, 3-, and 4-BisPEB and MPEP were built in Maestro (version 9.2; Schrödinger, LLC, New York, NY) and minimized in MacroModel (version 9.9; Schrödinger, LLC) with default settings. The backbone-dependent rotamer library included in PyMOL (PyMOL Molecular Graphics System, version 1.5; Schrödinger, LLC) was applied to Asn747 and Ser809 in our mGluR5 homology model (Kaae et al., 2012) to identify the most likely side-chain conformation for each residue with the hydrogen bonding donor groups pointing into the putative binding site. The receptor grids for docking in Glide (version 5.8; Schrödinger, LLC) were prepared as described previously (Kaae et al., 2012). 2-, 3-, and 4-BisPEB and MPEP were docked into the mGluR5 homology model using the XP scoring function with a scaling factor of 0.7 for all ligand atoms and asking for maximum 10 output poses. We selected the highest-ranking output poses that rationalize as much as possible of our and referenced mutational results as the most plausible binding modes.

Results

2-, 3-, and 4-BisPEB Displace [³H]MPEP. MPEP binds to an allosteric site in the 7TMD of mGluR5 (Pagano et al., 2000; Malherbe et al., 2003), and competitive binding studies
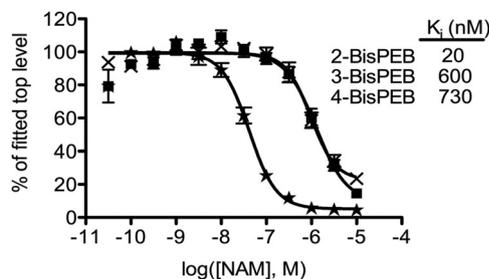
Fig. 2. 2-BisPEB (★), 3-BisPEB (■), and 4-BisPEB (✖) displace [³H]MPEP. This was shown by competitive binding studies on membrane prepared from BHK cells transiently transfected with wild-type mGluR5. The individual points represent means ± S.E.M. of normalized data pooled from two to three independent experiments (duplicate measurements) using one to two membrane batches. K_i was calculated using the Cheng-Prusoff equation and represent the mean from two to three independent experiments. K_D for [³H]MPEP was found to be 2.9 nM ($n = 3$) by saturation binding studies.

showed that all three BisPEBs can displace [³H]MPEP (Fig. 2) with relative affinities similar to the order of potencies found in the functional Ca^{2+} mobilization assay (Table 1). This finding is consistent with the three BisPEBs binding in the 7TMD like MPEP, which is further supported by the mutational data.

Mutational Studies. To elucidate the binding modes of the four NAMs, 14 residues were selected for mutation on the basis of the previously published docking of 2-BisPEB into our mGluR5 homology model (Kaae et al., 2012) and on previously published mutational data for MPEP (Pagano et al., 2000; Malherbe et al., 2003). The selected residues were either modeled by us to interact directly with 2-BisPEB, predicted to be located in close proximity to the suggested interaction partners, or found to have pronounced effects (≥ 10-fold) on the affinity and/or potency of MPEP or methoxy-MPEP in previous studies (Pagano et al., 2000; Malherbe et al., 2003). Complementing mutational strategies were designed to remove or introduce side chains with favorable and unfavorable interactions.

Mutational Effects on Cell Surface Expression, Glutamate Potency, and Efficacy. The mutants were characterized by transiently transfecting BHK cells with wild-type and mutant mGluR5 and measuring increases in intracellular Ca^{2+} concentration upon glutamate stimulation. The majority of the mutants responded to glutamate with efficacies and potencies not statistically significantly different from those of the wild type (E_{max} and EC_{50} values are given in Table 2). The mutants for which glutamate potency was significantly affected were T632P, R648E, W785A, and A810V (lower glutamate potency) and Y792A and A813F (higher glutamate potency). However, the differences were less than approximately 3-fold numerically. A cell surface ELISA was performed to investigate whether lower efficacy or lack of glutamate-stimulated response of some mutants was due to lower cell surface expression or non-/dysfunctional receptors. Optical density values are given in Table 2 as a measure for cell surface expression. The two nonresponding mutants (G628F and F788D) gave optical density responses comparable to those of mock transfected cells [0.072 ± 0.001 (mean ± S.E.M.), $n = 7$] indicating that the mutants were not expressed at the cell surface level in a sufficient amount to mediate a cellular response. It was found that the glutamate-stimulated response levels (rela-

tive E_{max}) in general correlated with cell surface expression of the mutants, giving a linear regression R^2 value = 0.81 (Supplemental Fig. 1).

Mutational Effects Common for All Four NAMs. To measure antagonistic activity, NAMs were automatically added to the cells expressing wild-type or mutant mGluR5 before stimulation with 10 μM L-glutamate (upper dynamic range of the concentration-response curves). When tested on the wild-type receptor, 2-BisPEB was >25 times as potent as the two other BisPEBs, although still approximately 10 times less potent than MPEP.

Four mutations (I651F, Y659A, F788W, and A810V) affected the potency of all four NAMs. The effect of I651F was strong for all four (>20-fold). The effect of Y659A was also strong, although the range was wider (14-fold for 2-BisPEB to 120-fold for MPEP). The effects of F788W and A810V were statistically significant for all NAMs but of varying magnitude. The effect of F788W ranged from >20-fold for 3- and 4-BisPEB to a modest 3.3-fold for 2-BisPEB; likewise the effect of A810V ranged from 63-fold for MPEP to 3.6-fold for 4-BisPEB. Five mutations (T632A, Y659F, G748L, Y792F, and A813F) displayed general minor effects and were therefore not considered of direct relevance for the interaction between any of the NAMs and mGluR5.

Mutations with Differential Effects on the Four NAMs. The largest effect for 2-BisPEB was seen when Ser809 was mutated. S809F and S809A resulted in a 63- and 19-fold decrease in potency, respectively. W785A and N747A both led to an 11-fold decrease in potency for 2-BisPEB, whereas N747S led only to a 5.4-fold decrease in potency. W785A decreased the potency of 2-BisPEB 11-fold. T632P and R648E had a potentiating effect of minor magnitude (IC_{50} ratio = 0.16 and 0.15, respectively, relative to that of the wild type).

Substantial effects on the potency of 3-BisPEB were seen for P655S (>20-fold), N747A (>20-fold), N747S (11-fold), and Y792A (>20-fold). The effect of R648E was statistically significant, but the shift in potency was only ~3-fold, and Arg648 is therefore not considered to be directly involved in the interactions between 3-BisPEB and mGluR5.

The only statistically significant mutation affecting 4-BisPEB potency without affecting the three other NAMs was F788A (~21-fold). The effects of W785A and Y792A were also statistically significant, but the shifts in potency were ~3-fold. W785A and Y792A are therefore not considered to be directly involved in the interactions between 3-BisPEB and mGluR5.

Of the mutations without a common effect on all tested NAMs, only one (N747A) was without a statistically significant effect on the potency of MPEP. For some of the other mutations, however, the effect on potency was of limited magnitude (7.4-fold for P655S, 4.2-fold N747S, and 8.1-fold for Y792A). As for 2-BisPEB, the two mutations T632P and R648E had a minor potentiating effect on MPEP-mediated inhibition of mGluR5 activity (IC_{50} ratio = 0.26 and 0.12, respectively, relative to that of the wild type). For other mutations, however, a relatively large decrease in potency was observed. These were W785A (280-fold), F788A (27-fold), S809F (490-fold), and S809A (52-fold).

Modeled Binding Modes of 2, 3-, and 4-BisPEB and MPEP. To put our experimental results into a structural context 2-, 3-, and 4-BisPEB and MPEP were docked into the

TABLE 1

Mutational effect on the potencies of 2-, 3-, and 4-BisPEB and MPEP

BHK cells were transiently transfected with wild-type and mutated mGluR5 using the calcium phosphate method. The intracellular Ca^{2+} response was measured on an imaging-based plate reader 2 days after transfection. The potency is presented as IC_{50} and pIC_{50} (mean ± S.E.M.) and represents data from n independent transfections and experiments (duplicate measurements). Mutants were compared with wild-type mGluR5 (pIC_{50}) by one-way ANOVA combined with Dunnett's multiple comparison test or by a one-sample t test for mutants with IC_{50} values ≥45 μM.

	2-BisPEB				3-BisPEB				4-BisPEB				MPEP			
	IC_{50}	IC_{50}/IC_{50} (wt)	pIC_{50}	n	IC_{50}	IC_{50}/IC_{50} (wt)	pIC_{50}	n	IC_{50}	IC_{50}/IC_{50} (wt)	pIC_{50}	n	IC_{50}	IC_{50}/IC_{50} (wt)	pIC_{50}	n
	nM		M		nM		M		nM		M		nM		M	
wt	79		7.10 ± 0.07	19	2200		5.66 ± 0.07	19	2100		5.67 ± 0.06	14	8.1		8.09 ± 0.05	19
T632A	83	1.1	7.08 ± 0.08	3	1800	0.90	5.75 ± 0.03	3	3500	1.7	5.45 ± 0.05	3	4.5	0.56	8.35 ± 0.02	3
T632P	13	0.16	7.9 ± 0.3***	3	790	0.35	6.1 ± 0.1	3	2500	1.2	5.61 ± 0.08	3	2.0	0.25	8.7 ± 0.1***	3
R648E	12	0.15	7.92 ± 0.03***	3	590	0.27	6.23 ± 0.08**	5	2000	1.0	5.7 ± 0.2	4	0.91	0.11	9.04 ± 0.06***	3
I651F	3200	41	5.5 ± 0.1***	3	>45,000	>20	—***	2	>45,000	>21	—***	2	500	62	6.3 ± 0.2***	3
P655S	160	2.0	6.8 ± 0.1	3	>45,000	>20	—***	2	3200	1.5	5.5 ± 0.1	6	60	7.4	7.22 ± 0.04***	3
Y659A	1100	14	5.97 ± 0.03***	3	1200	0.54	5.93 ± 0.09	3	>45,000	>21	—***	2	950	120	6.02 ± 0.03***	3
Y659F	38	0.48	7.42 ± 0.01	3	>45,000	>20	—***	2	630	0.30	6.2 ± 0.1*	3	5.5	0.68	8.26 ± 0.09	3
N747A	830	11	6.08 ± 0.07***	3	25,000	11	4.6 ± 0.2***	3	2800	1.3	5.55 ± 0.08	6	13	1.6	7.88 ± 0.06	3
N747S	430	5.4	6.37 ± 0.01***	3	4000	1.8	5.4 ± 0.3	3	5000	2.4	5.3 ± 0.1	3	34	4.2	7.47 ± 0.06***	3
G748L	79	1.0	7.1 ± 0.2	3	4300	2.0	5.37 ± 0.09[a]	3	4000	1.9	5.4 ± 0.1	3	40	4.9	7.4 ± 0.2***	3
W785A	890	11	6.05 ± 0.09***	3	1900	0.86	5.72 ± 0.06	6	6000	2.9	5.22 ± 0.09*	3	2300	280	5.64 ± 0.08***,[a]	3
F788A	98	1.2	7.01 ± 0.4	3	>45,000	>20	—***	2	~45,000	~21	—***	2	220	27	6.66 ± 0.06***	2
F788W	260	3.3	6.59 ± 0.09*	3	>45,000	>20	—***	3	>45,000	>21	—***	2	79	9.8	7.1 ± 0.2***	2
Y792A	160	2.0	6.79 ± 0.03	3	2500	1.1	5.6 ± 0.2	3	6300	3.0	5.20 ± 0.04*	3	66	8.1	7.18 ± 0.04***	3
Y792F	110	1.4	6.97 ± 0.04	3	6300	2.9	5.2 ± 0.2	3	1600	0.76	5.8 ± 0.1	3	13	1.6	7.90 ± 0.04	3
S809F	5000	63	5.3 ± 0.2***	3	2500	1.1	5.6 ± 0.2	3	5000	2.4	5.3 ± 0.1	3	4000	490	5.4 ± 0.1***	3
S809A	1500	19	5.81 ± 0.03***	6	>45,000	>20	—***	3	1000	0.48	6.0 ± 0.2	3	420	52	6.38 ± 0.09***	5
A810V	790	10	6.1 ± 0.1***	3	>45,000	>20	—***	3	7600	3.6	5.12 ± 0.08**	3	510	63	6.29 ± 0.04***	3
A813F	120	1.5	6.91 ± 0.08	3	3400	1.5	5.47 ± 0.07	3	3500	1.7	5.46 ± 0.03	3	10	1.2	7.99 ± 0.06	3

* $P < 0.05$.
** $P < 0.01$.
*** $P < 0.001$.
[a] Only partial inhibition of the glutamate response was observed.

TABLE 2

Mutational effect on glutamate-induced Ca^{2+}-response and cell surface expression of mGluR5

BHK cells were transiently transfected with wild-type and mutated mGluR5 using the calcium phosphate method. The intracellular Ca^{2+} response was measured on an imaging-based plate reader. Cell surface expression of wild-type and mutated receptors was determined by cell surface ELISA. Results are presented as mean ± S.E.M. and represent data from minimum two independent transfections. n states the number of experiments (duplicate measurements). Mutants were compared with wild-type mGluR5 (E_{max}, pEC_{50}, and OD) by one-way ANOVA combined with Dunnett's multiple comparison test.

		Relative E_{max}		Glutamate Potency			OD (Cell Surface ELISA)	
	Mutational Location	Mean ± S.E.M.	n	EC_{50}	pEC_{50}	n	Mean ± S.E.M.	n
		%		μM	M			
wt		100		1.0	6.00 ± 0.02	26	0.90 ± 0.04	6
G628F	TMH2	N.A.		N.A.			0.094 ± 0.004***	3
T632A	TMH2	58 ± 8**	3	1.8	5.75 ± 0.07	3	0.57 ± 0.03***	3
T632P	TMH2	67 ± 11**	4	1.8	5.74 ± 0.09*	4	0.72 ± 0.06*	3
R648E	TMH3	23 ± 4***	6	3.2	5.50 ± 0.08***	6	0.16 ± 0.01***	3
I651F	TMH3	105 ± 9	6	1.4	5.85 ± 0.05	6	0.93 ± 0.08	3
P655S	TMH3	77 ± 10*	6	1.4	5.85 ± 0.04	6	0.72 ± 0.02*	3
Y659A	TMH3	81 ± 9	6	1.0	6.02 ± 0.06	6	0.99 ± 0.05	3
Y659F	TMH3	91 ± 13	4	1.1	5.96 ± 0.05	4	0.78 ± 0.04	3
N747A	TMH5	93 ± 10	6	1.0	6.01 ± 0.04	6	0.84 ± 0.02	3
N747S	TMH5	108 ± 5	5	0.9	6.04 ± 0.05	5	0.76 ± 0.08	3
G748L	TMH5	100 ± 5	4	0.9	6.05 ± 0.07	4	0.94 ± 0.03	3
W785A	TMH6	59 ± 4***	6	2.5	5.60 ± 0.03***	6	0.54 ± 0.02**	3
F788A	TMH6	102 ± 13	5	1.4	5.86 ± 0.03	5	0.93 ± 0.03	3
F788D	TMH6	N.A.		N.A.			0.10 ± 0.01***	3
F788W	TMH6	84 ± 8	6	0.9	6.05 ± 0.05	6	0.74 ± 0.04	3
Y792A	TMH6	58 ± 2***	6	0.6	6.24 ± 0.06***	6	0.60 ± 0.05**	3
Y792F	TMH6	109 ± 3	5	1.0	6.00 ± 0.04	5	0.6 ± 0.1*	3
S809F	TMH7	37 ± 6***	5	1.3	5.89 ± 0.05	5	0.47 ± 0.06**	3
S809A	TMH7	85 ± 9	6	1.0	6.02 ± 0.03	6	0.6 ± 0.2	3
A810V	TMH7	92 ± 7	6	1.5	5.82 ± 0.04*	6	0.8 ± 0.1	3
A813F	TMH7	69 ± 6*	3	0.5	6.3 ± 0.2***	3	0.6 ± 0.1**	3

N.A., these mutants did not respond to glutamate (based on observations from a minimum of two independent transfections and experiments).

* $P < 0.05$.
** $P < 0.01$.
*** $P < 0.001$.

mGluR5 homology model to generate plausible binding modes that can rationalize the mutational results. Although asking for 10 output conformations, the extra-precision docking protocol used presented only four or fewer possible binding modes for each NAM. For 2-BisPEB we observed four different output poses and because only the second ranked pose was able to rationalize the most pronounced mutational effect, it was selected as the most likely binding conformation

(Fig. 3, a–c). For 3- and 4-BisPEB we observed very limited variation between the output poses, and the highest ranked poses were selected as potential binding modes (Fig. 3c). Docking of MPEP resulted in two completely different output poses; the highest-ranking pose (pose 1) was located between TMHs 3, 5, and 6 and the other pose (pose 2) in the area between TMHs 2, 3, 6, and 7 (Fig. 3d). Both MPEP poses are within interaction distance of approximately one-half of the
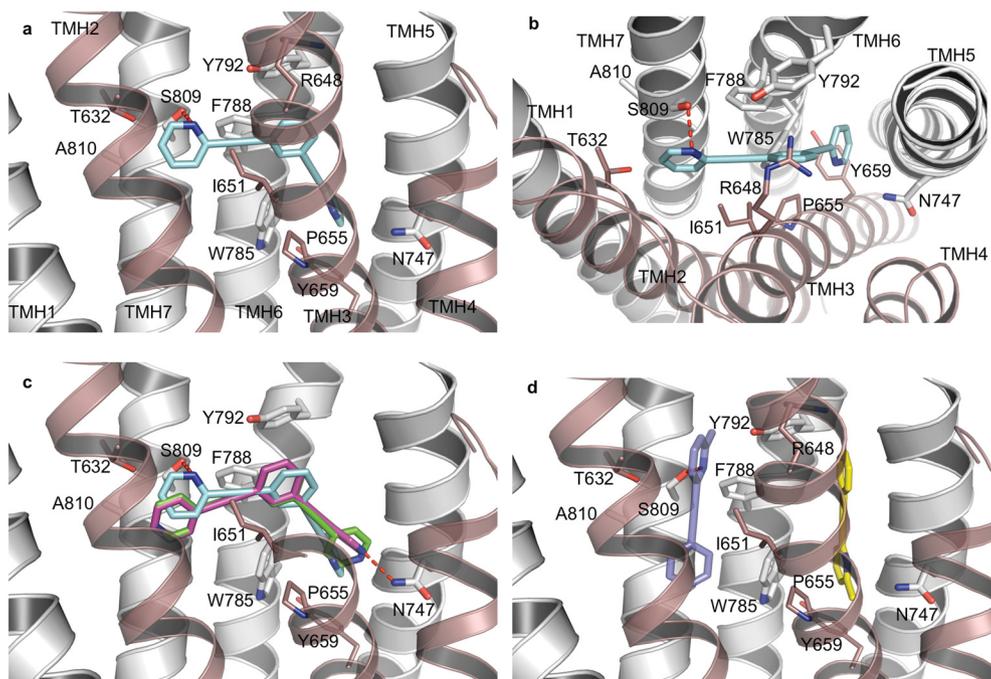

Fig. 3. Possible binding poses of the studied ligands obtained by molecular docking to the mGluR5 homology model selected by docking score and the number of mutations they can rationalize. a and b, suggested binding mode of 2-BisPEB (cyan carbons) in the 7TMD as seen from the side (membrane view) and from the top (extracellular view), respectively. c, comparison of the suggested binding modes of 2-BisPEB, 3-BisPEB (magenta carbons), and 4-BisPEB (green carbons). d, two possible binding poses of MPEP with the best scoring pose (pose 1, yellow carbons) between TMHs 3, 5, and 6 and the second ranked pose (pose 2, purple carbons) between TMHs 2, 3, 6, and 7. TMHs 1, 5, 6, and 7 are represented as white cartoon with the mutated residues discussed in the text shown as sticks. TMHs 2, 3, and 4 are represented as thin, transparent, and brown cartoon with residues discussed in the text shown as thin sticks. Dashed red lines indicate direct hydrogen bonds.

residues showing an effect on MPEP inhibition and therefore have similar plausibility. The three other NAMs, because of their larger size and bent shape, bridge both subsites, occupying a larger area between TMHs 2, 3, 5, 6, and 7. Thus, consistent with the results from the [^{3}H]MPEP binding assay, the potential binding conformations of all four compounds overlap (Fig. 3, c and d). The model with the docked compounds can be acquired by contacting the corresponding author.

Discussion

We set out to explain the large potency differences between three novel MPEP-derived mGluR5 NAMs with high structural similarity. We characterized the binding sites by combining extensive mutational studies with ligand docking into a homology model. Competitive binding studies showed that 2-, 3-, and 4-BisPEB can displace [^{3}H]MPEP, consistent with binding pockets located in the 7TMD. This result is further supported by mutations in the 7TMD affecting the potency of MPEP and 2-, 3-, and 4-BisPEB (Table 1) and the docking poses obtained (Fig. 3). Even though 2-, 3-, and 4-BisPEB are derived from MPEP (Kaae et al., 2012), their sizes and shapes result in binding modes distinct from that of MPEP. The mutational effects and structural interpretation of the BisPEBs and MPEP are therefore discussed separately.

Two mutations, I651F and Y659A, had pronounced effects on the potency of the three BisPEBs suggesting that these residues are involved in shaping the binding sites of all three NAMs. The mGluR5 homology model places Ile651 in the central part of the binding pockets (Fig. 3, a–c), and introducing a phenylalanine probably occludes the site hindering ligand binding. Tyr659 is placed in the bottom of the binding pocket between TMHs 3, 5, and 6, and our suggested binding modes indicate ligand-receptor π-π interactions with this residue, which is consistent with the fact that Y659F did not affect IC$_{50}$ of the BisPEBs, whereas Y659A increased IC$_{50}$ $\geq$14-fold.

Despite high structural similarity, 2-BisPEB was found to be >25 times as potent as 3- and 4-BisPEB. Given that the only structural difference is the nitrogen atom position in the pyridine rings (Fig. 1), the explanation for the varying potencies is likely to be found among hydrogen bonding partners. Residues Thr632, Arg648, Asn747, Tyr792, and Ser809 were identified as potential candidates on the basis of our previously published docking of 2-BisPEB (Kaae et al., 2012). The T632A, T632P, R648E, and Y792F mutations gave no indications of these residues being hydrogen bonding partners of any of the three BisPEBs (Table 1). However, mutation of two hydrophilic residues, Asn747 and Ser809, resulted in differential effects on the three BisPEBs (Table 1): the two Asn747 mutants primarily affected 3-BisPEB and to a minor degree 2-BisPEB, whereas the Ser809 mutations affected only 2-BisPEB. According to our docking studies, these effects can be explained by different hydrogen bonding patterns of the three BisPEBs based on the position of the pyridine nitrogens (Fig. 3c): only 2-BisPEB can form a direct hydrogen bond to Ser809, and the vicinity to Asn747 indicates a possible water-mediated hydrogen bond; 3-BisPEB can interact with Asn747 directly; and 4-BisPEB displays no hydrogen bonds. The mutational data as well as the docking studies suggest that the different interaction patterns to Ser809 are responsible for the higher potency of 2-BisPEB and result in a shifted bind-

ing mode for 2-BisPEB compared with that for 3- and 4-BisPEB (Fig. 3c). Thus, the S809A mutation is expected to result in a binding mode for 2-BisPEB similar to that of the two other NAMs, consistent with the similar IC$_{50}$ values for 2-BisPEB on the S809A mutant (1.5 μM) and 3-, and 4-BisPEB on the wild-type receptor (2.2 and 2.1 μM, respectively). Such a shift in binding mode would also allow introduction of bulk at residue 809 without a steric clash with the NAMs, explaining the relatively subtle effect of the S809F versus S809A mutation on 2-BisPEB ($\sim$3-fold), comparable with the effects of S809F versus wild type on 3- and 4-BisPEB (Table 1).

The different binding mode of the three BisPEBs also results in one of the pyridine rings of 2-BisPEB being closer to Trp785 and moves the central aromatic ring further away from Phe788 (Fig. 3c). Thus, the selective effect of W785A on 2-BisPEB may be explained by more optimal π-π interactions between Trp785 and 2-BisPEB compared with those on 3- and 4-BisPEB. The opposite may be true for mutations of Phe788, which affect only 3- and 4-BisPEB and not 2-BisPEB.

The P655S, Y792A, and A810V mutations, which also had differential effects on the BisPEBs, are more difficult to explain from our docking studies. Pro655 is located in the vicinity of Asn747 (Fig. 3) and because P655S affects the IC$_{50}$ of only 3-BisPEB, it could indicate that the serine introduced interacts with Asn747 and prevents the direct hydrogen bond to 3-BisPEB discussed above. Tyr792 is predicted to interact with the central aromatic ring of the BisPEBs and because the binding modes of 3- and 4-BisPEB overlap perfectly in this area (Fig. 3c), the model does not offer an explanation for the selective effect by Y792A on 3-BisPEB. Furthermore, none of the predicted binding modes (also applies to MPEP) display interactions to Ala810 (Fig. 3), and the occlusion of the binding site indicated by A810V remains unexplained by our model. This result indicates that TMH7 in mGluR5 may be slightly rotated compared with the class A GPCRs used as templates for our homology model. Such a rotation would, in addition to Ser809, also position Ala810 in the vicinity of the suggested binding poses, enabling the model to explain the mutational effects of the A810V mutation.

MPEP was included as a reference compound because the three BisPEBs were designed as MPEP analogs. Our molecular docking only returned two different potential MPEP binding poses; however, neither of the poses alone can rationalize the major mutational effects on MPEP potency: pose 1 is within favorable van der Waals contact distance of Pro655, Tyr659, Trp785, and Tyr792, whereas pose 2 is in contact with Ile651, Phe788, and Tyr792 and displays a hydrogen bond to Ser809 (Fig. 3d). Thus, each of the possible MPEP binding poses offers an explanation for the mutational effects of four residue positions, making them equally plausible. Detailed examination of the mGluR5 homology model shows that Trp785 divides the putative binding cavity into the two subsites occupied by the MPEP docking poses (Fig. 3d). This tryptophan is conserved in 73 and 69% of class C (including all mGluRs) and class A GPCRs, respectively. It is located in the middle of TMH6 and shapes the lower part of the 7TM binding cavity. Class A GPCRs have been explored by solving a number of crystal structures and so far the tryptophane has been shown to display only two different conformations (Cherezov et al., 2007; Rasmussen et al., 2007; Rosenbaum et

al., 2007; Jaakola et al., 2008; Warne et al., 2008; Chien et al., 2010; Wu et al., 2010; Shimamura et al., 2011; Haga et al., 2012). Both the Trp785 conformation incorporated in our mGluR5 model and the alternative conformation observed in one class A GPCR crystal structure (Haga et al., 2012) separate Tyr659 and Ser809 into different parts of the binding cavity. Both of these residues are suggested as important interaction partners for MPEP, as they were for 2-BisPEB, with Tyr659 as a potential π-π interaction partner and Ser809 as a potential hydrogen bonding partner. However, Trp785 makes it impossible to obtain a binding mode of MPEP that interacts directly with both residues.

The binding site of MPEP and that of a close structural analog, methoxy-MPEP, have been explored in two previous studies by similar approaches and with similar qualitative effects for identical or equivalent mutations (Pagano et al., 2000; Malherbe et al., 2003). However, both studies reported a single binding mode of MPEP based on their homology models that can rationalize all of their major mutational effects. Our homology model differs from those of Pagano et al. (2000) and Malherbe et al. (2003) by use of a sequence alignment based on all class A, B, and C GPCRs (Kaae et al., 2012); we use different templates and retain side chain conformations of conserved residues. Furthermore, as we make use of a validated docking program, as opposed to manual docking, it is not surprising that we obtain different binding modes for MPEP. The MPEP binding mode reported by Malherbe et al. (2003) is located just below Pro655 and Trp785 (Pro654 and Trp784 in the rat mGluR5 model of Malherbe et al., 2003) and is in contact with residues from both TMHs 5 and 7. However, in our model this area does not present a cavity that can accommodate MPEP. Pagano et al. (2000) reported a MPEP binding mode that interacts with both Tyr659 and Ser809 without the obstruction by Trp785. Such a binding mode is possible in their model because Tyr659 is located in the second helical turn of TMH3, compared with the fifth helical turn in our model, positioning Tyr659 and Ser809 much closer to each other without Trp785 in between.

Our mGluR5 homology model and predicted BisPEB binding modes show remarkably good consistency with our experimental data, suggesting that the model may be used to rationalize structure-activity relationship data for NAMs at mGluR5. However, the model and MPEP binding modes differ significantly from those reported previously, and two different MPEP binding modes are necessary to rationalize all the mutations with a significant effect on MPEP IC_{50}. A detailed explanation of the mode of action for MPEP inhibition is beyond the scope of this work, but our results could indicate that two different binding sites may exist. Another possible explanation could be that some of the residues showing an effect on MPEP inhibition, e.g., Ser809 and Ala810, do not affect binding but regulate access to the binding site as suggested previously (de Graaf and Rognan, 2009). That some residues are involved in early events in the ligand binding pathway but not in the final ligand binding has also been shown by molecular dynamics simulation studies (Dror et al., 2011).

In conclusion, we have identified nine residues, Ile651, Pro655, Tyr659, Asn747, Trp785, Phe788, Tyr792, Ser809, and Ala810, as important molecular determinants for the activity of the NAMs studied. Three of these residues, Ile651, Asn747, and Ser809, have not been implicated previously in

negative allosteric modulation of mGluR5, and Ser809, in particular, is highlighted as a potential important interaction partner. Our results show that the several-fold higher potency of 2-BisPEB compared with that of 3- and 4-BisPEB might be explained by a direct hydrogen bond between Ser809 and 2-BisPEB. The homology model used in the present study differs from other mGluR5 models published previously, but it can rationalize the structure-activity relations observed for the three BisPEB NAMs. Our model can also serve as starting point for studies of other NAMs, e.g., fenobam.

Authorship Contributions

Participated in research design: Mølck, Harpsøe, Pedersen, Nielsen, Mathiesen, and Bräuner-Osborne.
Conducted experiments: Mølck, Harpsøe, Gloriam, and Jimenez.
Contributed new reagents or analytic tools: Clausen and Madsen.
Performed data analysis: Mølck, Harpsøe, Gloriam, and Pedersen.
Wrote or contributed to the writing of the manuscript: Mølck, Harpsøe, Gloriam, Clausen, Madsen, Nielsen, Mathiesen, and Bräuner-Osborne.

References

Ballesteros J and Palczewski K (2001) G protein-coupled receptor drug discovery: implications from the crystal structure of rhodopsin. *Curr Opin Drug Discov Devel* **4:**561–574.
Bräuner-Osborne H, Wellendorph P, and Jensen AA (2007) Structure, pharmacology and therapeutic prospects of family C G-protein coupled receptors. *Curr Drug Targets* **8:**169–184.
Bridges TM and Lindsley CW (2008) G-protein-coupled receptors: from classical modes of modulation to allosteric mechanisms. *ACS Chem Biol* **3:**530–541.
Chen Y, Goudet C, Pin JP, and Conn PJ (2008) *N*-{4-Chloro-2-[(1,3-dioxo-1,3-dihydro-2*H*-isoindol-2-yl)methyl]phenyl}-2-hydroxybenzamide (CPPHA) acts through a novel site as a positive allosteric modulator of group 1 metabotropic glutamate receptors. *Mol Pharmacol* **73:**909–918.
Chen Y, Nong Y, Goudet C, Hemstapat K, de Paulis T, Pin JP, and Conn PJ (2007) Interaction of novel positive allosteric modulators of metabotropic glutamate receptor 5 with the negative allosteric antagonist site is required for potentiation of receptor responses. *Mol Pharmacol* **71:**1389–1398.
Cheng Y and Prusoff WH (1973) Relationship between the inhibition constant (K_1) and the concentration of inhibitor which causes 50 per cent inhibition (I_{50}) of an enzymatic reaction. *Biochem Pharmacol* **22:**3099–3108.
Cherezov V, Rosenbaum DM, Hanson MA, Rasmussen SG, Thian FS, Kobilka TS, Choi HJ, Kuhn P, Weis WI, Kobilka BK, et al. (2007) High-resolution crystal structure of an engineered human β_2-adrenergic G protein-coupled receptor. *Science* **318:**1258–1265.
Chien EY, Liu W, Zhao Q, Katritch V, Han GW, Hanson MA, Shi L, Newman AH, Javitch JA, Cherezov V, et al. (2010) Structure of the human dopamine D3 receptor in complex with a D2/D3 selective antagonist. *Science* **330:**1091–1095.
Christopoulos A, May LT, Avlani VA, and Sexton PM (2004) G-protein-coupled receptor allosterism: the promise and the problem(s). *Biochem Soc Trans* **32:**873–877.
Conn PJ, Lindsley CW, and Jones CK (2009) Activation of metabotropic glutamate receptors as a novel approach for the treatment of schizophrenia. *Trends Pharmacol Sci* **30:**25–31.
de Graaf C and Rognan D (2009) Customizing G protein-coupled receptor models for structure-based virtual screening. *Curr Pharm Des* **15:**4026–4048.
Dror RO, Pan AC, Arlow DH, Borhani DW, Maragakis P, Shan Y, Xu H, and Shaw DE (2011) Pathway and mechanism of drug binding to G-protein-coupled receptors. *Proc Natl Acad Sci USA* **108:**13118–13123.
Galambos J, Wágner G, Nógrádi K, Bielik A, Molnár L, Bobok A, Horváth A, Kiss B, Kolok S, Nagy J, et al. (2010) Carbamoyloximes as novel non-competitive mGlu5 receptor antagonists. *Bioorg Med Chem Lett* **20:**4371–4375.
Goudet C, Gaven F, Kniazeff J, Vol C, Liu J, Cohen-Gonsaud M, Acher F, Prézeau L, and Pin JP (2004) Heptahelical domain of metabotropic glutamate receptor 5 behaves like rhodopsin-like receptors. *Proc Natl Acad Sci USA* **101:**378–383.
Gregory KJ, Dong EN, Meiler J, and Conn PJ (2011) Allosteric modulation of metabotropic glutamate receptors: structural insights and therapeutic potential. *Neuropharmacology* **60:**66–81.
Haga K, Kruse AC, Asada H, Yurugi-Kobayashi T, Shiroishi M, Zhang C, Weis WI, Okada T, Kobilka BK, Haga T, et al. (2012) Structure of the human M2 muscarinic acetylcholine receptor bound to an antagonist. *Nature* **482:**547–551.

Jaakola VP, Griffith MT, Hanson MA, Cherezov V, Chien EY, Lane JR, Ijzerman AP, and Stevens RC (2008) The 2.6 angstrom crystal structure of a human A2A adenosine receptor bound to an antagonist. *Science* **322:**1211–1217.

Johnson KA, Conn PJ, and Niswender CM (2009) Glutamate receptors as therapeutic targets for Parkinson's disease. *CNS Neurol Disord Drug Targets* **8:**475–491.

Kaae BH, Harpsøe K, Kvist T, Mathiesen JM, Mølck C, Gloriam D, Jimenez HN, Uberti MA, Nielsen SM, Nielsen B, et al. (2012) Structure-activity relationships for negative allosteric mGluR5 modulators. *ChemMedChem* **7:**440–451.

Kunishima N, Shimada Y, Tsuji Y, Sato T, Yamamoto M, Kumasaka T, Nakanishi S, Jingami H, and Morikawa K (2000) Structural basis of glutamate recognition by a dimeric metabotropic glutamate receptor. *Nature* **407:**971–977.

Malherbe P, Kratochwil N, Mühlemann A, Zenner MT, Fischer C, Stahl M, Gerber PR, Jaeschke G, and Porter RH (2006) Comparison of the binding pockets of two chemically unrelated allosteric antagonists of the mGlu5 receptor and identification of crucial residues involved in the inverse agonism of MPEP. *J Neurochem* **98:**601–615.

Malherbe P, Kratochwil N, Zenner MT, Piussi J, Diener C, Kratzeisen C, Fischer C, and Porter RH (2003) Mutational analysis and molecular modeling of the binding pocket of the metabotropic glutamate 5 receptor negative modulator 2-methyl-6-(phenylethynyl)-pyridine. *Mol Pharmacol* **64:**823–832.

Mühlemann A, Ward NA, Kratochwil N, Diener C, Fischer C, Stucki A, Jaeschke G, Malherbe P, and Porter RH (2006) Determination of key amino acids implicated in the actions of allosteric modulation by 3,3′-difluorobenzaldazine on rat mGlu5 receptors. *Eur J Pharmacol* **529:**95–104.

Muto T, Tsuchiya D, Morikawa K, and Jingami H (2007) Structures of the extracellular regions of the group II/III metabotropic glutamate receptors. *Proc Natl Acad Sci USA* **104:**3759–3764.

Nakanishi S and Masu M (1994) Molecular diversity and functions of glutamate receptors. *Annu Rev Biophys Biomol Struct* **23:**319–348.

Niswender CM and Conn PJ (2010) Metabotropic glutamate receptors: physiology, pharmacology, and disease. *Annu Rev Pharmacol Toxicol* **50:**295–322.

Noetzel MJ, Rook JM, Vinson PN, Cho HP, Days E, Zhou Y, Rodriguez AL, Lavreysen H, Stauffer SR, Niswender CM, et al. (2012) Functional impact of allosteric agonist activity of selective positive allosteric modulators of metabotropic glutamate receptor subtype 5 in regulating central nervous system function. *Mol Pharmacol* **81:**120–133.

Pagano A, Ruegg D, Litschig S, Stoehr N, Stierlin C, Heinrich M, Floersheim P, Prezèau L, Carroll F, Pin JP, et al. (2000) The non-competitive antagonists 2-methyl-6-(phenylethynyl)pyridine and 7-hydroxyiminocyclopropan[*b*]chromen-1*a*-carboxylic acid ethyl ester interact with overlapping binding pockets in the transmembrane region of group I metabotropic glutamate receptors. *J Biol Chem* **275:**33750–33758.

Palucha A and Pilc A (2007) Metabotropic glutamate receptor ligands as possible anxiolytic and antidepressant drugs. *Pharmacol Ther* **115:**116–147.

Pin JP, Galvez T, and Prézeau L (2003) Evolution, structure, and activation mechanism of family 3/C G-protein-coupled receptors. *Pharmacol Ther* **98:**325–354.

Rasmussen SG, Choi HJ, Rosenbaum DM, Kobilka TS, Thian FS, Edwards PC, Burghammer M, Ratnala VR, Sanishvili R, Fischetti RF, et al. (2007) Crystal structure of the human β_2 adrenergic G-protein-coupled receptor. *Nature* **450:**383–387.

Ritzén A, Sindet R, Hentzer M, Svendsen N, Brodbeck RM, and Bundgaard C (2009) Discovery of a potent and brain penetrant mGluR5 positive allosteric modulator. *Bioorg Med Chem Lett* **19:**3275–3278.

Rosenbaum DM, Cherezov V, Hanson MA, Rasmussen SG, Thian FS, Kobilka TS, Choi HJ, Yao XJ, Weis WI, Stevens RC, et al. (2007) GPCR engineering yields high-resolution structural insights into β_2-adrenergic receptor function. *Science* **318:**1266–1273.

Shimamura T, Shiroishi M, Weyand S, Tsujimoto H, Winter G, Katritch V, Abagyan R, Cherezov V, Liu W, Han GW, et al. (2011) Structure of the human histamine H1 receptor complex with doxepin. *Nature* **475:**65–70.

Spooren W and Gasparini F (2004) mGlu5 receptor antagonists: a novel class of anxiolytics? *Drug News Perspect* **17:**251–257.

Swanson CJ, Bures M, Johnson MP, Linden AM, Monn JA, and Schoepp DD (2005) Metabotropic glutamate receptors as novel targets for anxiety and stress disorders. *Nat Rev Drug Discov* **4:**131–144.

Tsuchiya D, Kunishima N, Kamiya N, Jingami H, and Morikawa K (2002) Structural views of the ligand-binding cores of a metabotropic glutamate receptor complexed with an antagonist and both glutamate and Gd^{3+}. *Proc Natl Acad Sci USA* **99:**2660–2665.

von Zastrow M and Kobilka BK (1994) Antagonist-dependent and -independent steps in the mechanism of adrenergic receptor internalization. *J Biol Chem* **269:**18448–18452.

Warne T, Serrano-Vega MJ, Baker JG, Moukhametzianov R, Edwards PC, Henderson R, Leslie AG, Tate CG, and Schertler GF (2008) Structure of a β_1-adrenergic G-protein-coupled receptor. *Nature* **454:**486–491.

Wellendorph P and Bräuner-Osborne H (2009) Molecular basis for amino acid sensing by family C G-protein-coupled receptors. *Br J Pharmacol* **156:**869–884.

Wu B, Chien EY, Mol CD, Fenalti G, Liu W, Katritch V, Abagyan R, Brooun A, Wells P, Bi FC, et al. (2010) Structures of the CXCR4 chemokine GPCR with small-molecule and cyclic peptide antagonists. *Science* **330:**1066–1071.

Zhang P, Zou MF, Rodriguez AL, Conn PJ, and Newman AH (2010) Structure-activity relationships in a novel series of 7-substituted-aryl quinolines and 5-substituted-aryl benzothiazoles at the metabotropic glutamate receptor subtype 5. *Bioorg Med Chem* **18:**3026–3035.

Zheng L, Baumann U, and Reymond JL (2004) An efficient one-step site-directed and site-saturation mutagenesis protocol. *Nucleic Acids Res* **32:**e115.

Address correspondence to: Dr. Hans Bräuner-Osborne, Department of Drug Design and Pharmacology, Faculty of Health and Medical Sciences, University of Copenhagen, Fruebjergvej 3, DK-2100 Copenhagen. E-mail: hbo@sund.ku.dk